RSC Advances

ROYAL SOCIETY OF CHEMISTRY

www.rsc.org/advances

RSC Advances

RSC Publishing

ARTICLE

Effect of growing Graphene flakes on branched carbon nanofibers based on carbon fiber on mechanical and thermal properties of polypropylene

Cite this: DOI: 10.1039/x0xx00000x

Received ooth January 2012,
Accepted ooth January 2012

DOI: 10.1039/x0xx00000x

www.rsc.org/

Ferial Ghaemi,[a] Ali Ahmadian,[b] Robiah Yunus,[*a] Mohamad Amran Mohd Salleh, [a] and Nurazak Senu [b]

A one-step process, the chemical vapor deposition method, has been used to fabricate graphene flakes (G) on branched carbon nanofibers (CNF) grown on carbon fibers (CF). In this contribution, the G-CNF-CF fibers have been used as reinforcing fillers in a polypropylene (PP) matrix in order to improve the mechanical and thermal properties of the PP. A bimetallic catalyst (Ni/Cu) was deposited on a CF surface to synthesize branched CNF using C_2H_2/H_2 precursors at 600°C followed by growing G flakes at 1050°C. The morphology and chemical structure of the G-CNF-CF fibers were characterized by means of electron microscopy, transmission electron microscopy, and Raman spectroscopy. The mechanical and thermal behaviors of the synthesized G-CNF-CF/PP composite were characterized by means of tensile tests and thermal gravimetric analysis. Mechanical measurements revealed that the tensile stress and Young's modulus of the G-CNF-CF/PP composites were higher than the neat PP with the contribution of 76%, 73%, respectively. Also, the thermal stability of the resultant composite increased about 100°C. The measured reinforcement properties of the fibers were fitted with a mathematical model obtaining good agreement between the experimental results and analytical solutions.

Abbreviations: Carbon fiber, CF; Carbon nanofiber, CNF; Carbon nanotube, CNT; Graphene, G; Chemical vapour deposition, CVD; Polypropylene, PP; Scanning electron microscopy, SEM; Transmission electron microscopy, TEM; field emission scanning electron microscopy, FESEM; Thermal gravimetric analysis, TGA.

Introduction

Carbon fiber (CF) has been widely used in various industry fields because of its high strength and low weight, and also its ability to reinforce a composite [1]. A low portion of this filler in the polymer composite has revealed remarkable improvement of the thermal and mechanical properties [2-4]. The properties of composite materials depend not only on the reinforcing fillers and polymer matrix but also on the interfacial adhesion between them. High interfacial adhesion provides the strong structure of composites with an effective load transfer from the polymer matrix to the fiber. Polymeric composites based on carbon nanomaterials, such as carbon nanofiber (CNF), carbon nanotube (CNT) and graphene (G) with the excellent properties, have attracted tremendous attention due to their excellent physical and mechanical properties [5-12]. The

CNFs can act as rod-shaped fillers and enhance the polymer properties in the polymer composite [13-15]. G with a two-dimensional structure and honeycomb lattice has been widely studied since it was discovered by Novoselove et al. [16]. This nanomaterial has the potential to be applied in both scientific research and industrial applications because of its remarkable characteristics in terms of the mechanical, thermal and electrical properties [17]. Additionally, G was investigated as an outstanding reinforcing filler to compose a composite with good dispersion [18-24].

Furthermore, the synthesis of carbon nanomaterials on CF has been reported to increase the surface area of CF in order to improve the interfacial adhesion between the fiber and the matrix [25-27]. Hence, the carbon nanomaterials, such as G and CNF, on CF fabricate a robust network with a polymer matrix to enhance the interfacial properties of composites [28].

To provide large-scale production with a low dimension and high purity, as an important issue in advanced nanomaterial research, the CVD technique has been investigated [29] and applied to fabricate CNF and then G [30-33]. It has been found that the morphology of synthesized carbon nanomaterials depends on the reaction parameters of the CVD process (e.g., growth time, growth temperature and also catalyst solution) [34-37].

The catalyst solution has a critical role to synthesize the branched CNFs and also the G layers. Several studies have been carried out by using Ni or Cu as catalysts to grow CNF and G. To synthesize high quality graphene, CVD on Cu is considered as one of the most distinguishing methods because of its fabrication in a large-area and a single-layer garphene [38-42]. In addition, Ni is one of the most widely studied catalysts for the synthesis of graphene [43,44] and carbon nanaofibers [45,46] because a strong Ni–C interaction causes a repulsive interaction within the C–C interaction and causes the dissolution at the edge of a graphene [47]. However, limited research has been devoted to the usage of a bimetallic catalyst (Ni/Cu) to synthesize G and CNF. The Ni/Cu alloy is an excellent binary system to control carbon solubility by tuning the atomic fraction of Ni in Cu. Robinson et al. exploited foils of this binary system (Ni/Cu) to produce a G film [48] which was followed by Yan-Li and co-authors to use the Ni-Cu alloy to grow high strength CNF [49]. The hybrid of the CNFs and G films has been synthesized by Dai and co-workers by using the plasma enhanced CVD method on Cu as a substrate to obtain a three-dimensional (3D) carbon architecture [50].

On the other hand, polypropylene (PP) is a thermoplastic polymer and can be made by polymerizing propylene molecules. PP has been attained a considerable attention as a preferred reinforcing polymer since it is a member of the group of commodity thermoplastics synthesized in large quantities and not very responsive to chemical stress cracking. Regarding the several useful properties like high heat distortion temperature, transparency, flame resistance and dimensional stability, PP frequently was used as a matrix material for composite fabrication [51].

To the best of our knowledge, so far nobody has reported any work being widely carried out on synthesizing G layers on the branched CNF grown on CF by using a bimetallic catalyst (Ni/Cu) in a one-step CVD method in order to increase the CF surface area.

In this research, the produced G-CNF-CF was incorporated into a PP matrix to fabricate the composite (G-CNF-CF/PP). Furthermore, the effects of the G-CNF coated phase on the CF surface were investigated in terms of the mechanical and thermal properties of the PP composite. To this end, a tensile test as well as thermal gravimetric analysis (TGA) was applied. The surface morphology and structural characterization of the samples were analyzed through scanning electron microscopy (SEM), transmission electron microscope (TEM) and Raman spectroscopy.

Experimental

Materials

In this work, unsized CF (Toho Tenax Co. Ltd.) was activated by immersing it in nitric acid (65%). Besides that, a high purity acetylene (C2H2) as a carbon source, nitrogen (Air Product, 99.9995) as a carrier gas, and copper nitrate trihydrate ($Cu(NO_3)_2.3H_2O$) and nickel nitrate hexahydrate ($Ni(NO_3)_2.6H_2O$) as catalyst sources were utilized in the experimental part. Polypropylene pellets (PP 600G) were bought from Petron at the Polymer Marketing and Trading Division, Malaysia and utilized as the polymer matrix.

Synthesis of Branched CNFs and G

The carbon fibers were immersed into a mixture of copper nitrate trihydrate and nickel nitrate hexahydrate solution (70%, 30%) and followed by ultrasonic agitation for 2h. Then they were dried and calcinated at 200°C under air flow for 2h to remove the nitrate components and make the desired catalyst coating on the surface of the CF. CVD was applied to grow the CNFs on the CF at atmospheric pressure and the temperature at 600°C for 30min. This process was fulfilled by a catalytic reaction of an acetylene flow rate of 50 standard cubic centimeters per minute (sccm) over Ni-Cu/CF in the reactor under a flow rate of H_2/N_2 (100, 100 sccm). At the end of the run time, the C_2H_2 flow was stopped, the heater was turned off and then the reactor was cooled under the flow of N_2. This heating process was repeated again to branch the CNFs. After that, the temperature was increased to 1050°C under H_2/N_2 (100, 100 sccm) and then the acetylene (50sccm) was inserted into the reactor for 30min to obtain the graphene layers. The schematic representation of the G growth on the CNFs has been indicated in Fig. 1. Investigation of the structural characterization of the resulting G and CNF was fulfilled by Raman spectroscopy. Besides that, the morphology of the product was inspected through a scanning electron microscope (SEM) and transmission electron microscope (TEM).

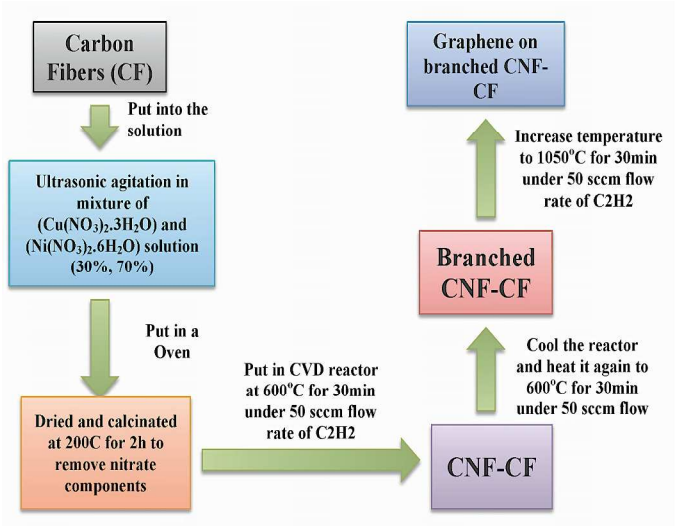

Fig. 1 Scheme diagram of graphene growth on branched CNF synthesized on CF surface.

Composites preparation

To prepare the composite, polypropylene (PP) was melted and blended in a mixer (Thermo Haake Poly Drive R600/ 610) at 180˚C with a 55rpm rotor speed for 5min and then mixed with fibers (5 wt. %) and blended for 15min [52]. The blended composite was put in a mold of the size 15×15 cm with a1mm thickness, allowed to melt at 180˚C under a pressure of 150 kg/cm^2 by way of a HSINCHU Hot Press Machine and then cooled to 60˚C.

Mechanical and thermal testing

The specimen with a thickness of 1mm was cut into bone shapes according to the ASTM D638 standard [53]. A tensile test was performed by using an Instron Universal Testing Machine at room temperature to measure the modulus of elasticity and the strength of PP, CF/PP, CNF–CF/PP and G–CNF–CF/PP. The tests were carried out with a crosshead speed of 5 mm/min [54]. Moreover, a thermal gravimetric analysis (TGA) test was employed to determine the thermal stability and degradation resistance of the nanoparticle composites [55]. TGA was fulfilled on a Mettle Stare SW 9.10 thermal gravimetric analyzer. First of all, the sample (0.65 mg) was put in the specimen holder and heated to 200˚C for a few minutes to remove the water. Then, the heating program started from 25˚C to 900˚C with a10˚C/min heating rate under a nitrogen flow.

Results and discussion

Structural characterization

The SEM image of the pristine CF has been presented in Fig. 2 (a) with 5–6 μm and 500 μm in diameter and length, respectively. The synthesized CNFs, formed by the adsorption and decomposition of the carbon source, have been demonstrated in Fig. 2 (b). Fig. 2 (c) depicts a SEM image of a G–CNF on the CF surface with intertwined branches of CNFs. The micrographs in Fig. 3 show a CNF and its structure.

TEM was employed to capture images of the G–CNF-CF. The sample was dispersed in an acetone solution in order to separate the nanoparticles from each other. The TEM image in Fig. 3 (a) reveals the branches of CNFs with entangled structures. As marked by arrows, some branches of the CNFs have the same diameters with the pristine CNF and some of them have smaller diameters. In Fig. 3 (b), the TEM image of CNF appears as the herringbone structure. Enlarged field emission scanning electron microscopy (FESEM) and TEM images of the fishbone-shape CNF with a dendritic nanostructure covered by flake-shaped graphenes have been displayed in Fig 4 (a) and (b), respectively. The TEM image indicates that the graphene flakes not only adhered to the CNF but were also directly bonded to the CNF surface. The graphene sheets with 200-1000 nm widths are presented in Fig. 5. From Fig. 5(c), it can be found that the G flake was composed of a few graphene layers.

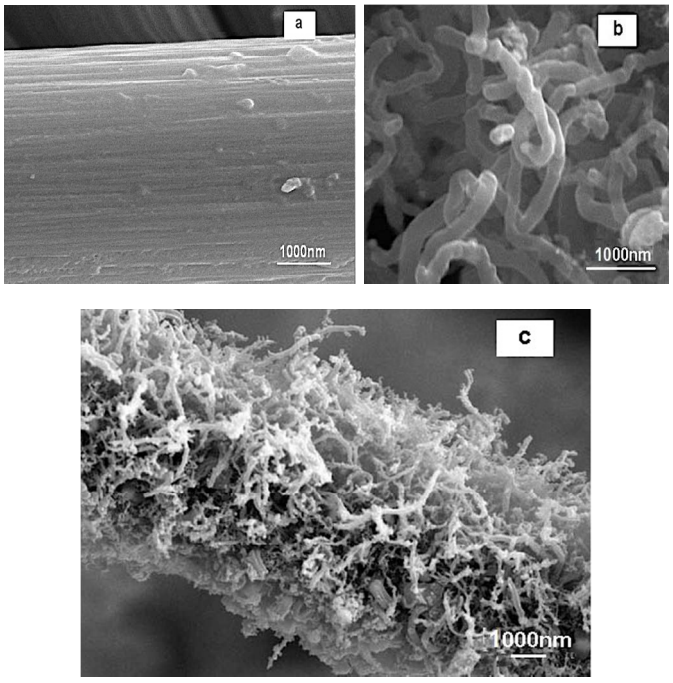

Fig. 1 SEM images of (a) pristine CFs, (b) grown CNFs and (c) G layers on branched CNF coated CF.

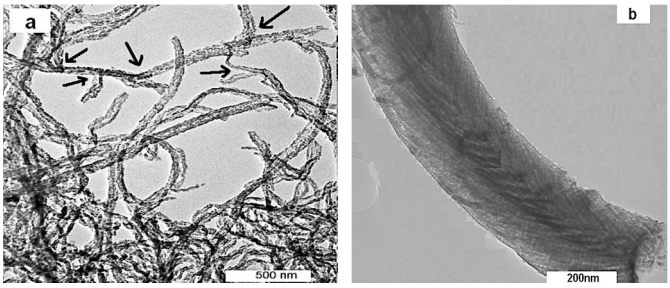

Fig. 2 TEM images of the (a) branched CNFs and (b) herringbone structure of CNF.

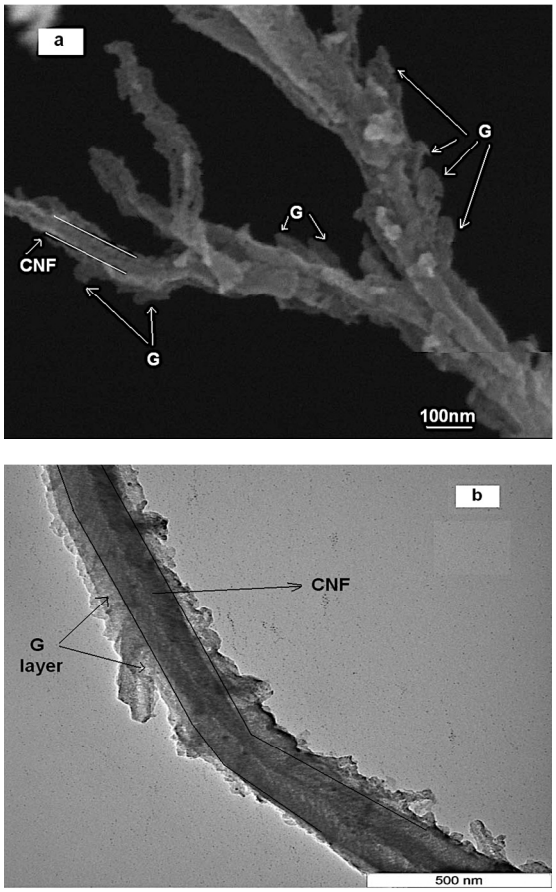

Fig. 3 (a) FESEM and (b) TEM images of the G on CNFs.

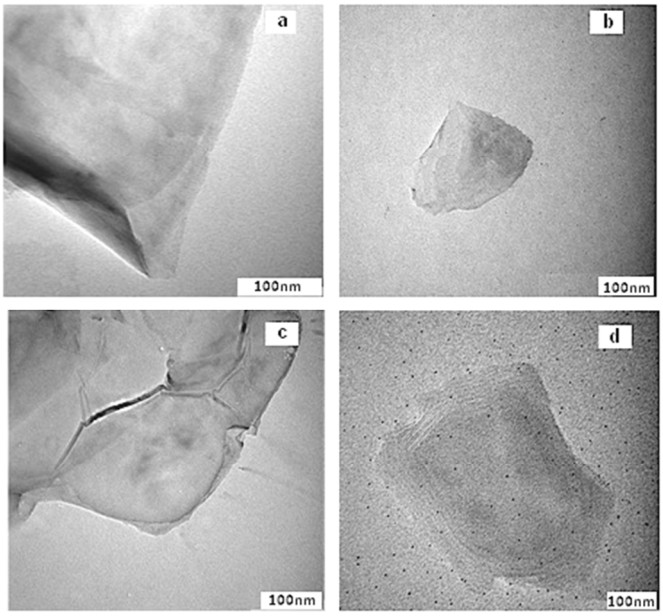

Fig. 4 TEM images of the (a), (b), (c) G flakes and (d) G composed of few graphene layers.

Raman spectroscopy is widely applied to structural characterization and quality information of the produced carbon nanoparticles [56]. The Raman spectra in Fig. 6 show a simple characterization of the resulting CNF, G on CF surface and their interaction with PP. Fig. 6 (a) was taken from the branched CNF-CF surface, while the spectrum in Fig. 6 (b) was taken from the G-CNF-CF sample. In these spectra, three peaks have been observed, D peak (~1350 cm^{-1}), G peak (~1580 cm^{-1}) and 2D peak (~2650cm^{-1}). The D peak relates to the breathing modes of the sp^2 atom [57], which is activated by the presence of any defect (e.g., lattice disorder [58], edges or functional groups [59]). The G peak is associated with an E_{2g} stretching mode of the graphitic crystalline structure. The intensity ratio of the D peak and the G peak (I_D /I_G) was utilized to evaluate the degree of graphitization [59].

Besides, Raman spectroscopy was used to explain the influence of the fillers on the mechanical behaviour of the composite. Fig. 6(c) shows a Raman spectrum of pure PP and Fig. 6(d) reveals the Raman spectrum of the composite. The Raman spectra confirm the strong interaction between the filler and PP matrix. The presence of this strong interaction is due to the CF-CNF-G as filler in the PP matrix. To compare the CF-CNF-G/PP with neat PP, one can see the location of D peak and 2D peak shows no changes whereas the small shift of the G peak was observed for this composite in which the PP chains were grafted onto graphene surface through covalent bonds [60]. It has been found that the frequency of G peak can be tuned by the mechanical properties of filler [61].

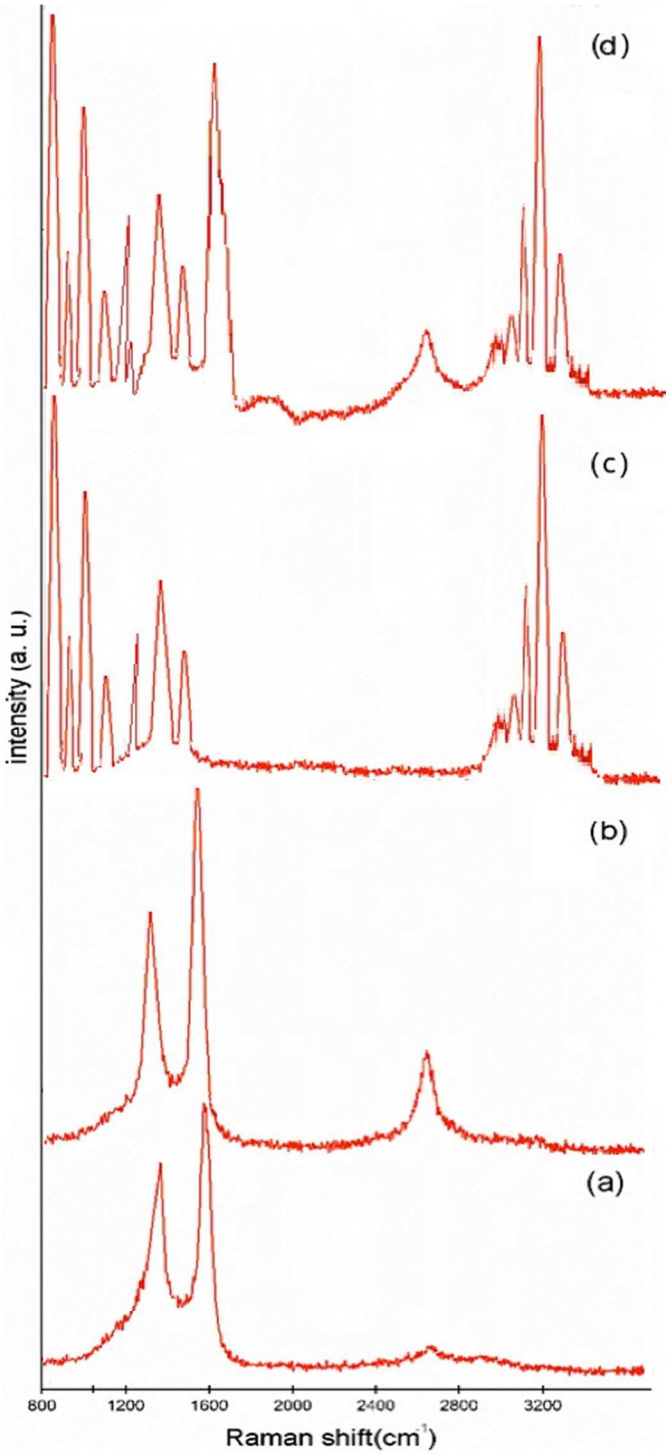

Fig. 5 Typical Raman spectra from (a) CF-CNF, (b) CF-CNF-G, (c) neat PP and (d) CF-CNF-G/PP composite

Mechanical and thermal tests

According to Table 1 and Fig. 7, the tensile stress of the unreinforced matrix would be enhanced by incorporating carbon fiber with carbon nanofiber and also graphene. In addition, comparison of the stiffness of the composite fabricated from CNF-CF and G-CNF-CF with neat CF illustrates a significant improvement in the tensile modulus. The reduction of the tensile stress and Young's modulus at the uncoated CF-PP composite was related to the defective flow of the matrix around the neat carbon fiber that caused decreased interfacial properties, and was easily pulled out of the carbon fiber from the matrix [62]. Similar to the stiffness, the strength of the CNF-CF/PP and G-CNF-CF/PP composites was higher than with the CF-PP composite because of the presence of CNF and G that led to the improvement of the stress transfer between the CF and the matrix [63].

Table 1. Tensile results for different composites (with 5 wt.% filler- 95 wt.% PP

Samples	Tensile stress (MPa)	Increase (%)	Young's modulus (MPa)	Increase (%)
PP	14.6 ± 0.3	-	479.8 ± 18.7	-
CF/PP	20.5 ± 0.5	40%	592.7 ± 24.5	23%
Branched CNF-CF/PP	23.7± 0.8	62%	704.2 ± 30.5	46%
G-CNF-CF/PP	25.8± 0.6	76%	830.1± 34.1	73%

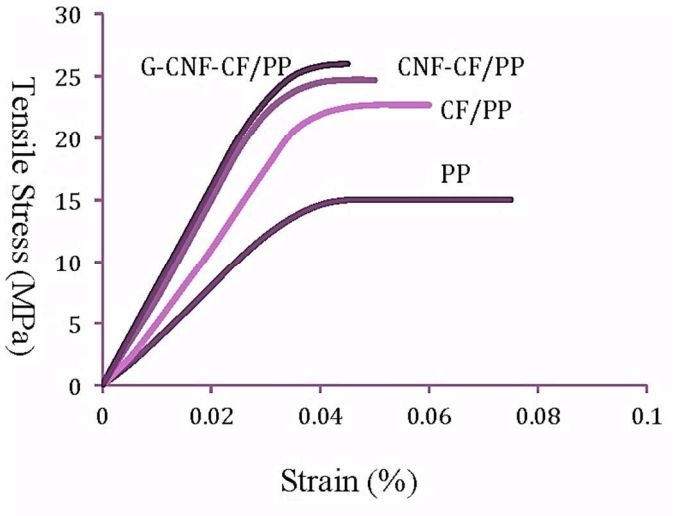

Fig. 7 Graph of tensile stress–starin of PP, CF/PP, CNF-CF/PP and G-CMF-CF/PP (with 5 wt.% filler- 95 wt. % PP).

The relationship between the mechanical properties of the composites and the reinforcement fillers has been systemically investigated. Mathematical models can be used to predict the mechanical properties of composites. The Halpin–Tsai (HT)

equation is an accepted and extensively adopted model to estimate the stiffness of fiber/polymer composites [64]. The HT model correlates the stiffness of the composite with the tensile modulus of the matrix and reinforcement as well as its volume contents and geometry. This model has been developed to calculate the tensile modulus of composites with unidirectional or randomly distributed fibers.

In this calculation, CF, CNF-CF and G-CNF-CF were assumed as fillers with a random distribution in the polypropylene matrix. By considering the incorporation of G-CNF with CF reinforcements within the matrix, the HT equations can be modified according to the following equation [65]:

$$E_c = \frac{3}{8}V_f E_f + \frac{5}{8}V_m E_m \qquad (1\text{-}1)$$

where E_c is the modulus of the composite; E_f is the Young's modulus of the filler; V_f is the filling content of the filler; E_m is the Young's modulus of the polymer matrix and V_m is the filling content of the polymer matrix.

Then, the effective reinforcement modulus of the fillers can be obtained as below:

$$E_f = \frac{E_c - \frac{5}{8}V_m E_m}{\frac{3}{8}V_f} \qquad (1\text{-}2)$$

Based on equation (1-2), the Young's modulus of the various fillers was calculated and reported in Fig. 8, where Ec was collected from Table 1, E_m was about 479.8 MPa, V_f was 5% and V_m was 95%.

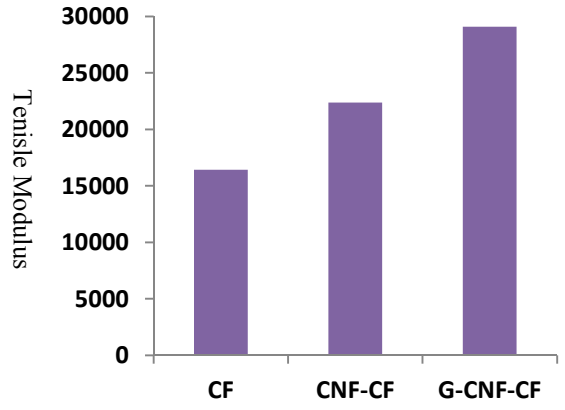

Fig. 8 Effective reinforcement modulus of different fillers in polypropylene matrix.

According to Fig. 8, it was found that the modulus of G-CNF-CF was higher than the other fillers. Such a meaningful difference is related to the not only uniform and excellent catalyst coating but also the maximum reaction time to synthesis. By comparing the Young's modulus of fibers, it can be deduced that the presence of graphene flakes on the CNF surface enhanced the tensile modulus of the CF, significantly. The difference in the effective reinforcement modulus between CNF-CF and G-CNF-CF were about 6715 MPa, which was higher than the difference between CNF-CF and CF (5947 MPa). Hence, the impact of the graphene layer was more than the carbon nanofibers to reinforce the polymer. Consequently, the mathematical predictions confirm the experimental results of the tensile modulus of the fillers.

The fracture behaviors of the CF/PP, CNF-CF/PP and G-CNF-CF/PP composites were studied after the tensile test as it has depicted under the SEM micrograph in Fig. 8. The typical fractured surface of the PP composites with neat CF, CNF-CF and G-CNF-CF have been displayed in Fig. 9 (a), (b) and (c), respectively. It can be found that the neat CFs with a smooth surface had minimal signs of any interfacial interaction with the polymer matrix. In the case of the CNF-CF/PP composite, some interactions of the PP residue to the CF surface have appeared as indicated by the relatively rough surface of the fillers. The presence of great amounts of PP matrix on the CF surface shown in Fig. 7 (c) is proof of the enhanced adhesion between the fiber and the PP matrix. Such interaction can be interpreted as affecting grafting of not only CNF on CF but also G on the CNF surface. Besides that, the micromechanical coupling of the fillers with the matrix is related to the effective PP matrix transfusion into the G-CNF on the CF surfaces, which led to a strong interlocking matrix with the fillers.

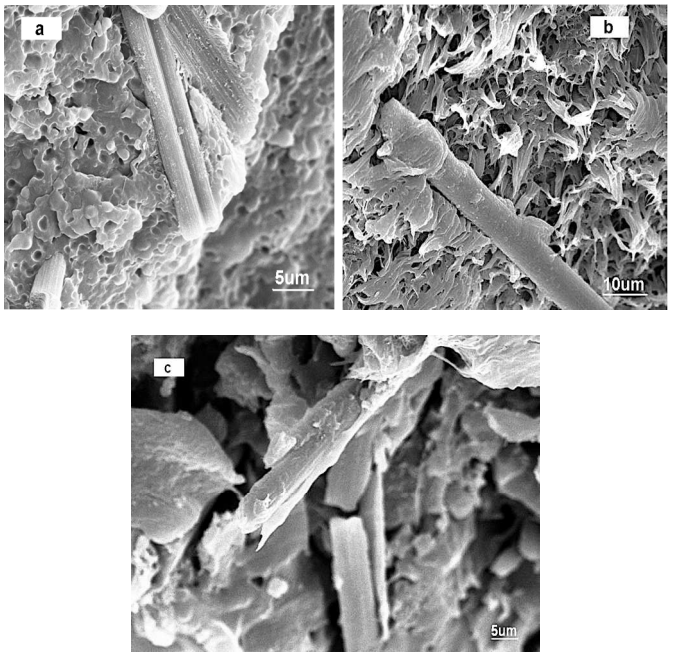

Fig. 6 SEM images of fractured surface of (a) CF/PP, (b) CNF-CF/PP and (c) G-CNF-CF/PP composites

TGA curves present a single degradation step for all samples and also thermal degradation began to occur after the materials absorbed a certain amount of heat. The heat causes the degradation process that led to the breakdown of the matrix structure of the sample. This curve demonstrates the TGA profiles of the samples according to the weight loss of the samples (%) versus temperature (°C). The TGA curves of the pure PP, CF/PP, CNF-CF/PP and G-CNF-CF/PP composites are shown in Fig. 10. The presence of fillers, such as CF, CNF and G layers to the PP matrix caused an increase in the composite degradation temperature because of having a high heat absorption capacity. The CF/PP composite lost weight at 350°C; that was higher than the pure PP. On the other hand, the CNF-CF/PP composite was evaluated by the mass losses during the TGA at temperatures between 400°C and 500°C. The mass losses at temperatures above 400°C were related to the decomposition of CNF while the mass losses below this temperature corresponded to the amorphous carbon materials [66]. It could be generally seen that for the G-CNF-CF/PP sample, there was no change in weight of the sample until the temperature reached around 450°C. This weight loss was related to the oxidation of the nanographene layer coating on the CNF which began to degrade around 450°C and completely degraded around 600°C. Therefore, by growing a garphene layer on the CNF, the thermal stability of the polymer composite is increased in comparison with the CNF-CF/PP and CF/PP composites.

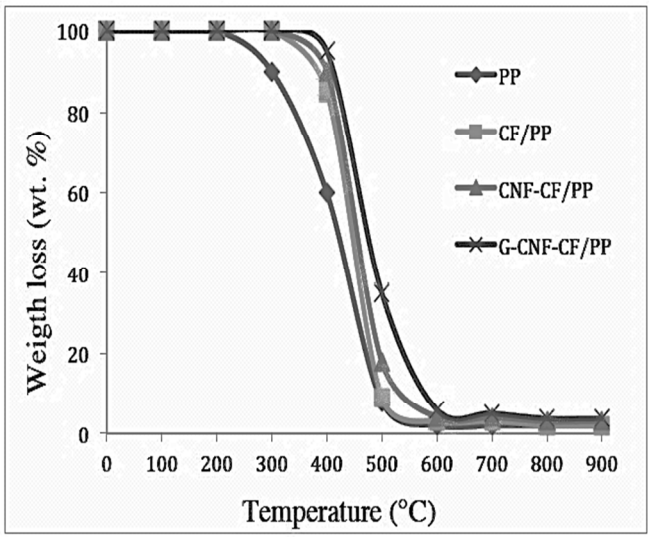

Fig. 7 TGA curves of the different composites

Conclusions

The most important contribution of this research is related to modifying the surface of CF through growing CNF-G in order to use as fillers in the PP matrix to enhance the mechanical and thermal properties of the PP composite. It can be understood that the one-step CVD method was able to grow CNF-G on the CF surface by using a bimetallic catalyst (Ni/Cu). The synthesis of the G flakes on the branched CNFs grown on the CF surface is a significant part of the current study that acts as a robust network to increase the surface adhesion between the CF and the matrix, which leads to improving the properties of the polymer composites. In order to evaluate the effects of the CNF/G coating on the CF surface in terms of mechanical and thermal properties, the tensile test and TGA were performed on the G-CNF-CF/PP, CNF-CF/PP and CF/PP composites. Since the G-CNF-CF/PP composite has a strong structure, the tensile stress and young's modulus of the G-CNF-CF/PP compared to the neat PP have increased 76% and 73%, respectively. According to the effective reinforcement, which was predicted by the mathematical model, it was found that the graphene has a main role rather than other fillers. This was verified by comparing the tensile modulus of different fillers. In addition to that, the thermal degradation resistance of the G-CNF-CF/PP increased by roughly 100°C in comparison with the CF/PP.

Acknowledgements

The authors gratefully acknowledge the financial support given by Universiti Putra Malaysia (UPM) under the Exploratory Research Grant Scheme (ERGS).

Notes and references

[a] Institute of Advanced Technology (ITMA), Universiti Putra Malaysia, 43400 UPM, Serdang, Selangor, Malaysia
[b] Department of Mathematics, Faculty of Sciences, Universiti Putra Malaysia, 43400 UPM, Serdang, Selangor, Malaysia

* Corresponding Author (E-mail: robiah@upm.edu.my Tel: +60122306009)

1 Q. Zhang, J. Liu, R. Sager, L. Dai and J. Baur, Composites Science and Technology, 2009, **69**, 594–601.
2 H. Mahfuz, A. Adnan, V. K. Rangari, S. Jeelani and B. Z. Jang, Composites Part A, 2004, **35**, 519–527.
3 F. Rezaei, R. Yunus, N. A. Ibrahim and E. S. Mahdi, Polymer-Plastics Technology and Engineering, 2008, **47**, 351–357.
4 S. Aziz, S. Abdul Rashid, S. Rahmanian and M. A. Salleh, POLYMER COMPOSITES, 2014.
5 A. Khattab, C. Liu, W. Chirdon and C. Hebert, Journal of Thermoplastic Composite Materials, 2012, **26**, 954–967.
6 M. H. Al-Saleh, G. A. Gelves and U. Sundararaj, Materials & Design, 2013, **52**, 128–133.
7 S. Bal, Materials & Design, 2010, **31**, 2406–2413.
8 S. Stankovich, D. A. Dikin, G. H. B. Dommett, K. M. Kohlhaas, E. J. Zimney, E. A. Stach, R. D. Piner, S. B. T. Nguyen and R. S. Ruoff, Nature, 2006, **442**, 282-286.
9 J. N. Coleman, U. Khan, W. J. Blau and Y. K. Gun'ko, Carbon, 2006, **44**, 1624-1652.

10 I. M. Inuwa, Azman Hassan, S. A. Samsudin, M. K. Mohamad Haafiz, M. Jawaid, K. Majeed, N. C. Abdul Razak, Journal of Applied Polymer Science, 2014, **131**.
11 L. Chen, H. Jin, Z. Xu, M. Shan, X. Tian, C. Yang, Z. Wang and B. Cheng, Materials Chemistry and Physics, 2014, **145**, 186-196.
12 F. Ghaemi, A. Amiri and R. Yunus, Trends in Analytical Chemistry, 2014, **59**, 133–143.
13 R. M. Novais, J. A. Covas and M. C. Paiva, Composites Part A, 2012, **43**, 833–841.
14 M. C. Paiva, R. M. Novais, R. F. Arau´jo, K. K. Pederson, M. F. Proenc¸ C. J. R. Silva, C. M. Costa and S. Lanceros-Me´ ndez, Polymer Composites, 2010, **3**, 369-376.
15 R. J. Foster, P. J. Hine and I. M. Ward**,** Polymer, 2009, **50**, 4018–4027.
16 K.S. Novoselov, A.K. Geim, S.V. Morozov, D. Jiang, Y. Zhang, S.V. Dubonos, I.V.Grigorieva and A.A. Firsov, Science, 2004, **306**, 666–669.
17 Y. Zhang, L. Zhang, C. Zhou, Accounts of Chemical Research, 2013, **46,** 2329-2339.
18 M. J. Allen, V. C. Tung and R. B. Kane, Chemical reviews, 2009, **110**, 132-135.
19 Y. Si and E. T. Samulski, Nano letters, 2008, **6**, 1679-1682.
20 D. Cai and M. Song, Journal of Materials Chemistry, 2010, **37**, 7906-7915.
21 H. Kim, A. A. Abdala C. W. Macosko, Macromolecules, 2010, **16**, 6515-6530.
22 T. Kuilla, S. Bhadra D. Yao, N. H. Kim, S. Bose and J. H. Lee, Progress in Polymer Science, 2010, **11**, 1350-1375.
23 R. Sengupta, M. Bhattacharya S. Bandyopadhyay and A. K. Bhowmick, Progress in Polymer Science, 2011, **5**, 638-670.
24 S. Stankovich, D. A. Dikin, G. H. B. Dommett, K. M. Kohlhaas, E. J. Zimney and E. A. Stach, Nature, 2006, **442**, 282-286.
25 H. Qian; E. S. Greenhalgh, M. S. P. Shaffer and A. Bismarck, Journal of Materials Chemistry, 2010, **20**, 4751-4762.
26 S. Tiwari, J. Bijwe and S. Panier, Tribology Letters, **2011**, 42, 293–300.
27 S. Tiwari, J. Bijwe and S. Panier. Journal of Materials Science, 2012, **47**, 2891–2898.
28 J. Liang, M. C. Saha, M. C. Altan, Procedia Engineering, 2013, **56**, 814 – 820.
29 F. Ghaemi, R. Yunus, M. A. M. Salleh, H. N. Lim, S. A. Rashid, Fullerenes, Nanotubes and Carbon Nanostructures, **DOI:** 10.1080/1536383X. 2014. 951439.
30 S. Liu, Z. Zhou, Z. Lin, Q. Ouyang, J. Zhang, S. Tian, M. Xing, BMC Biochemistry, 2009, **10**, 22.
31 N. Lisi, R. Giorgi, M. Re, T. Dikonimos, L. Giorgi, E. Salernitano, S. Gagliardi, F. Tatti, Carbon, 2011, **49**, 2134 –2140.
32 S. Zhu, Q. Li, Q. Chen, W. Liu, X. Li, J. Zhang, Q. Wang, X. Wang and H. Liu, RSC Advances, 2014, **4**, 32941- 32945.
33 A. H. Loo, A. Ambrosi, A. Bonanni and M. Pumera, RSC Advances, 2014, **4**, 23935-23952.
34 E. T. Thostenson, W. Z. Li, D. Z. Wang, Z. F. Ren, Journal of Applied Physics, 2002, **91**, 6034-6037.
35 Z. Fan, C. Wu, J. Chen, S. Yi, *Carbon,* **2008**, 46, 365-.380.
36 S. Zhu, C. H. Su, S. L. Lehoczky, I. Muntele, D. Ila, Diamond and Related Materials, 2003, **12**, 1825-1828.
37 Z. G. Zhao, L. G. Ci, H. M. Cheng, J. B. Bai, Carbon, 2005, **43**, 651-653.
38 X. Li, W. Cai, J. An, S. Kim, S. Nah, D. P. R. Yang, Science, 2009, **324**, 1312–1314.
39 C. Mattevi, H. Kim and M. Chhowalla, Journal of Materials Chemistry, 2011, **21**, 3324–34.
40 A. Venugopal, J. Chan, X. Li, C. W. Magnuson, W. P. Kirk and L. Colombo. Journal of Applied Physics, 2011,**109**, 104511-104515.
41 D. A. C. Brownson and C. E. Banks, Physical Chemistry Chemical Physics, 2012, **14**, 8264-8281.
42 Y. P. Hsieh, M. Hofmann and J. Kong, Carbon, 2014, **67**, 417–423.
43 C. M. Seah, S. P. Chai and A. R. Mohamed, Carbon, 2014, **70**, 1–21.
44 J. L. Qi, W. T. Zheng**,** X. H. Zheng, X. Wang and H. W. Tian, Applied Surface Science , 2011, **257**, 6531–6534.
45 M. A. Davoodi, J. Towfighi and A. Rashidi, Chemical Engineering Journal, 2013, **221**, 159–165.
46 E. Kimmari, V. Podgursky, M. Simunin, E. Adoberg, A. Surženkov, M. Viljus, M. Hartelt, R. Wäsche, I. Sildos and P. Kulu, Surface and Coatings Technology, 2013, **225**, 21–25.
47 K. Takahashi, K. Yamada, H. Kato, H. Hibino and Y. Homma. Surface Science, 2012, **606**, 728–32.
48 Z. R. Robinson, P. Tyagi, T. M. Murray, C. A. Ventrice Jr, S. Chen, A. Munson, C. W. Magnuson and R. S. Ruoff, ournal of Vacuum Science and Technology A, 2012, **30**, 011401.
49 W. Yan-li, W. Xu-jian, Z. Liang, Q. Wen-ming, L. Xiao-yi and L. Li-cheng, New Carbon Materials, 2012, **27**, 53–156.
50 G. P. Dai, M. H. Wu, D. K. Taylor, M. K. Brennamanc and K. Vinodgopal, RSC Advances, 2012, **2**, 8965–8968.
51 Q. TH. Shubhra, A. Alam, M. A. Quaiyyum, Journal of Thermoplastic Composite Materials, 2011, **26**, 362-391.
52 F. Rezaei, R. Yunus and N. A. Ibrahim, Materials and Design, 2009, **30**, 260–263.
53 ASTM D638. Standard test method for tensile properties of plastics. West Conshohocken (PA): ASTM International; 2010
54 S. Y. Fu, B. Lauke, E. Mader, C. Y. Yue, X. Hu. Composites Part A: Applied Science and Manufacturing, 2000, **31**, 1117–25.
55 M. S. Vishkaei, M. A. M. Salleh, R. Yunus, D. R. A. Biak, F. Danafar and F. Mirjalili, Journal of Composite Materials, 2010, 1–7.
56 H. C. Hsu, C. H. Wang, S. K. Nataraj, H. C. Huang, H. Y. Du, S. T. Chang, L. C. Chen and K. H. Chen, Diamond and Related Materials, 2012, **25**, 176-179.
57 L. G. Cancado, A. Jorio, E. H. Martins Ferreira, F. Stavale, C. A. Achete, R. B. Capaz, M. V. O.Moutinho, A. Lombardo, T. S. Kulmala and A. C. Ferrari, Nano Letters, 2011, **11**, 3190–3196.
58 A. C. Ferrari, D. M. Basako, Nature Nanotechnology, 2013, **8**, 235-246.
59 J. Y. Hwang, C. C. Kuo, L. C. Chen and K. H. Chen, Nanotechnology, 2010, **21**, 465705.
60 M. C. Hsiao, S. H. Liao, Y. F. Lin, C. A. Wang, N. W. Pu, H. M. Tsai, C. C. M. Ma, Nanoscale, 2011, **3**, 1516-1522.
61 T. M. G. Mohiuddin, A. Lombardo, R.R. Nair, A. Bonetti, G. Savini, R. Jalil, A. C. Ferrari, Physical Review B, 2009, **79,** 205433.
62 S. Rahmanian, K. S. Thean, A. R. Suraya, M. A. Shazed, M. A. M. Salleh and H. M. Yusoff, Materials and Design, 2013, **43**, 10–16.
63 R. J. Sager, P. J. Klein, D. C. Lagoudas, Q. Zhang, J. Liu, L. Dai and J. W. Baur, Composites Science and Technology, 2009, **69**, 898–904.

64 J. C. Halpin, J. L. Kardos, Polymer Engineering and Science, 1976, **16**, 344-352.
65 M. A. Shazed, A R. Suraya, S. Rahmanian, M. A. Mohd Salleh, Materials and Design, 2014, **54**, 660–669.
66 E. Mansfield, A. Kar and S. Hooker, Analytical and bioanalytical chemistry, 2010, **396**, 1071-1077.